

## RESEARCH ARTICLE

10.1029/2018SW001933

### Special Section:

Space Weather Events of 4–10  
September 2017

#### Key Points:

- Solar flare events can have a significant impact on GNSS positioning
- The critical effects are based on rapid changes of the dayside ionosphere during the peak phase of the flare event
- The knowledge of the flare spectrum is very important in order to estimate its significance for GNSS users

#### Correspondence to:

J. Berdermann,  
jens.berdermann@dlr.de

#### Citation:





Berdermann, J., Kriegel, M., Banyś, D., Heymann, F., Hoque, M. M., Wilken, V., et al. (2018). Ionospheric response to the X9.3 Flare on 6 September 2017 and its implication for navigation services over Europe. *Space Weather*, 16. <https://doi.org/10.1029/2018SW001933>

Received 1 MAY 2018

Accepted 28 SEP 2018

Accepted article online 4 OCT 2018

# Ionospheric Response to the X9.3 Flare on 6 September 2017 and Its Implication for Navigation Services Over Europe

J. Berdermann<sup>1</sup> , M. Kriegel<sup>1</sup> , D. Banyś<sup>1</sup>, F. Heymann<sup>1</sup>, M. M. Hoque<sup>1</sup>, V. Wilken<sup>1</sup>, C. Borries<sup>1</sup> , A. Heßelbarth<sup>1</sup>, and N. Jakowski<sup>1</sup> 

<sup>1</sup>German Aerospace Center, Neustrelitz, Germany

**Abstract** On 6 September 2017, an X-class flare of the magnitude 9.3 occurred around noon UT, being the strongest flare event in a decade. The flare itself was the highlight of a quite interesting phase of solar-terrestrial interactions caused by the active region known as the Catania sunspot group 46 or active region number 2673 on the NOAA catalog. From 3 to 13 September 2017 strong flare activities occurred, accompanied by a number of radio bursts and earthward-directed coronal mass ejections. Solar wind influences at Earth were modest during the flare activity and limited to the polar regions (Linty et al., 2018, <https://doi.org/10.1029/2018SW001940>). But, the strong X9.3 flare itself had impacts on the dayside ionosphere causing some problems in navigation services as we present within this paper. The event data observed and analyzed give us the opportunity to improve our understanding of strong and extreme space weather events and allow us to distinguish between the influence of the different event classes on our technological infrastructure within periods of strong solar activity. Here we will discuss our observations with special focus on the X9.3 flare event and provide examples how the flare itself influenced services in the domains of aviation and maritime navigation in the European sector.

## 1. Introduction

Space weather with all its temporal and spatial variations in the ionosphere is becoming an increasing threat to the precision of Global Navigation Satellite System (GNSS)-based navigation services needed in aviation or predictable future applications like automated car navigation. Next to the effects of nominal space weather changes, which are mainly of interest in certain business domains, strong solar events can cause a huge impact on different areas of daily life. Space weather events can be roughly separated into the categories moderate, strong, and extreme, based on the strength and its impact on infrastructure. There is a decrease in the occurrence frequency with increasing impact strength of the space weather event. Still, the likelihood of an extreme event within the next decade is not negligible and has been estimated with about 12% (Riley, 2012; Riley & Love, 2017). The class of extreme events in particular is still poorly understood with regard to its impact on our modern society. Due to the rather limited statistics of <0.01 extreme events per solar cycle and the rather limited time of about 400 years of solar observation in comparison to the age of the Earth and solar-terrestrial interaction, we do not know their maximum possible strength and impact. The limited information of such events allows only a very rough idea of the direct impact on the technical infrastructure and related costs (Eastwood et al., 2017; Oughton et al., 2017) and cannot estimate the costs of all the secondary effects on our daily life.

The direct effects of space weather on the technological infrastructure can be broadly defined in terms of the impact on the large electrically conducting infrastructure, malfunction of space and ground assets, space radiation, impacts on satellite drag, and direct impact on radio wave and other communication transmissions (Schrijver et al., 2015). Therefore, any new information which allows us to improve our knowledge of extreme space weather and their interaction with our infrastructure and services is of utmost interest. We must be prepared for a huge event at any time as has been concluded from the findings of Baker et al. (2013), who investigated the large coronal mass ejection (CME) in July 2012, which hit the STEREO-A (Solar Terrestrial Relations Observatory) spacecraft of the National Aeronautics and Space Administration at the Sunside facing away from Earth. The author predicted that the 2012 event could have had enormous technological impacts on Earth, but luckily missed it by about a week of solar rotation. At the moment we have rather poor statistics of extreme events such as the Carrington event in 1859, where almost no ground and no space

©2018. The Authors.

This is an open access article under the terms of the Creative Commons Attribution-NonCommercial-NoDerivs License, which permits use and distribution in any medium, provided the original work is properly cited, the use is non-commercial and no modifications or adaptations are made.

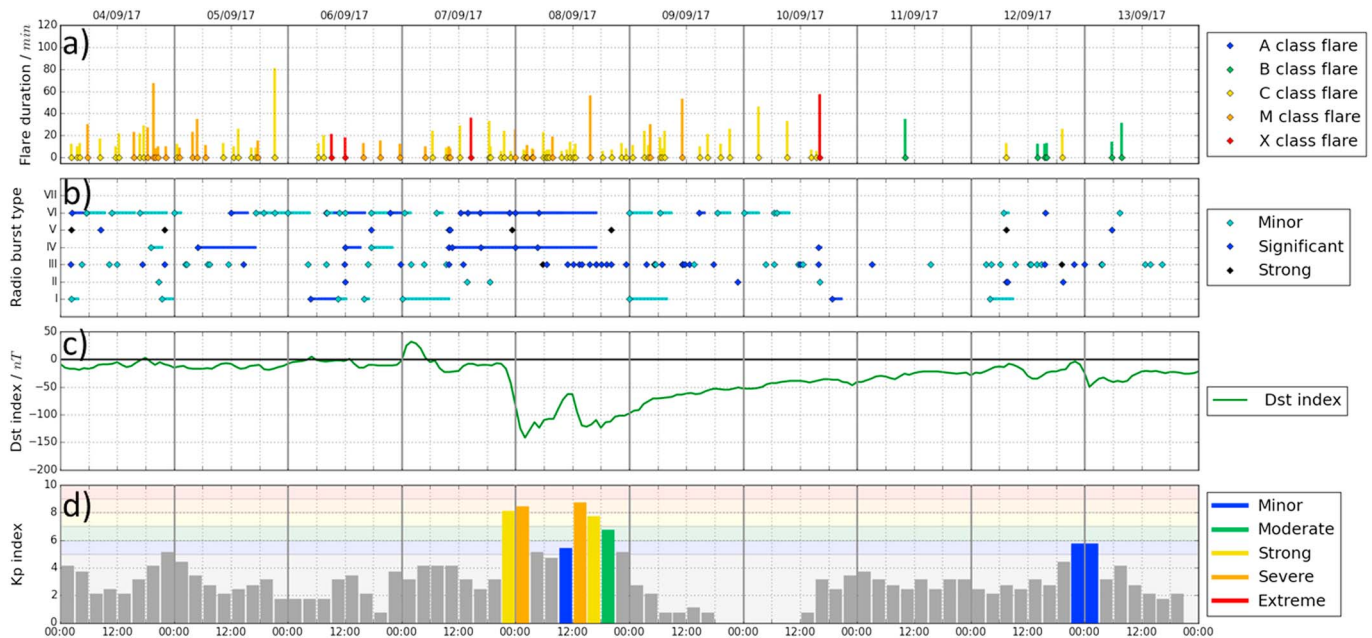


**Figure 1.** Time series of the solar and geomagnetic activity during 4 till 13 September 2017. The Figure shows from top to bottom: The flare activity with its classification and duration (a), the radio burst activity with its type and duration (b), the global geomagnetic indices Dst (c), and Kp (d). Flare and radio burst event data are provided by NOAA—Space Weather Prediction Center, Dst by World Data Center for Geomagnetism, Kyoto and Kp by GFZ Potsdam as member of the International Service of Geomagnetism.

infrastructure existed, and the 2012 event, which does not hit the Earth at all. We must therefore use information from moderate and strong space weather events for risk assessment and development of mitigation means. Particularly strong events can provide an insight into the threat situation that an extreme event can induce to our technological infrastructure.

In September 2017 a quite interesting period of solar activity occurred with an X9.3-class flare, the strongest solar flare in more than a decade, during its maximum phase (Chamberlin et al., 2018; Gimenez de Castro et al., 2018). The period from 3 to 13 September 2017 gave us an insight into solar-terrestrial interaction and allowed us to study its influence on navigation in more detail. In the following we will start with a brief description of the interesting solar activity period.

On 3 September 2017, the Catania group 46 (NOAA active region 2673) region started to grow and evolve into a magnetically complex structure for several days causing a series of solar flares, radio bursts, and CMEs (Redmon et al., 2018). As can be seen in Figure 1, the whole period can be divided into three phases. The first activity phase, where the sun spot group produced several M flares and short radio bursts, started early on 4 September and lasted till 5 September 9:00 UT. The strongest flare event of this phase was in the order of M5.5, reaching its peak on 4 September at 20:33 UT. The flare caused an Earth-directed CME, measured by a moderate change of the solar wind conditions on 6 September at about 11:00 UT. The CME caused some moderate ionospheric disturbances visible in the polar region, which will be briefly discussed in section 2.

In Figure 1 we can see that the first phase is followed by a short period of inactivity during the evening hours of 5 September before the main phase of activity started on 6 September. The main phase, starting around 6:00 UT on 6 September and lasting till 18:00 UT on 10 September, contains two major flare events on 6 September, an X2.2 at 9:10 UT and an X9.3 at 11:53 UT as well as strong radio burst activity over a wide range of the frequency spectrum (Figures 1a and 1b). These two strong solar flares have been recorded by different instruments in different spectral ranges as illustrated in Figure 2. This figure offers a detailed view of the ground-based Very Low Frequency (VLF) amplitude recorded by DLR's (German Aerospace Center) Global Ionospheric Flare Detection System (cf. Figure 2a), the satellite measurements in the X-ray range provided by the Geostationary Observational Environmental Satellite (GOES; cf. Figure 2b, data by NGDC, <https://ngdc.noaa.gov/>), and the EUV flux measured by the Solar Dynamic Observatory (SDO; cf. Figure 2c, data by LASP, <http://lasp.colorado.edu/>). Figure 2a presents the direct impact of the two flare events on the lower dayside ionosphere (see the blue curve for the disturbed day on 6 September and the black curve for an exemplary quiet day). Since VLF

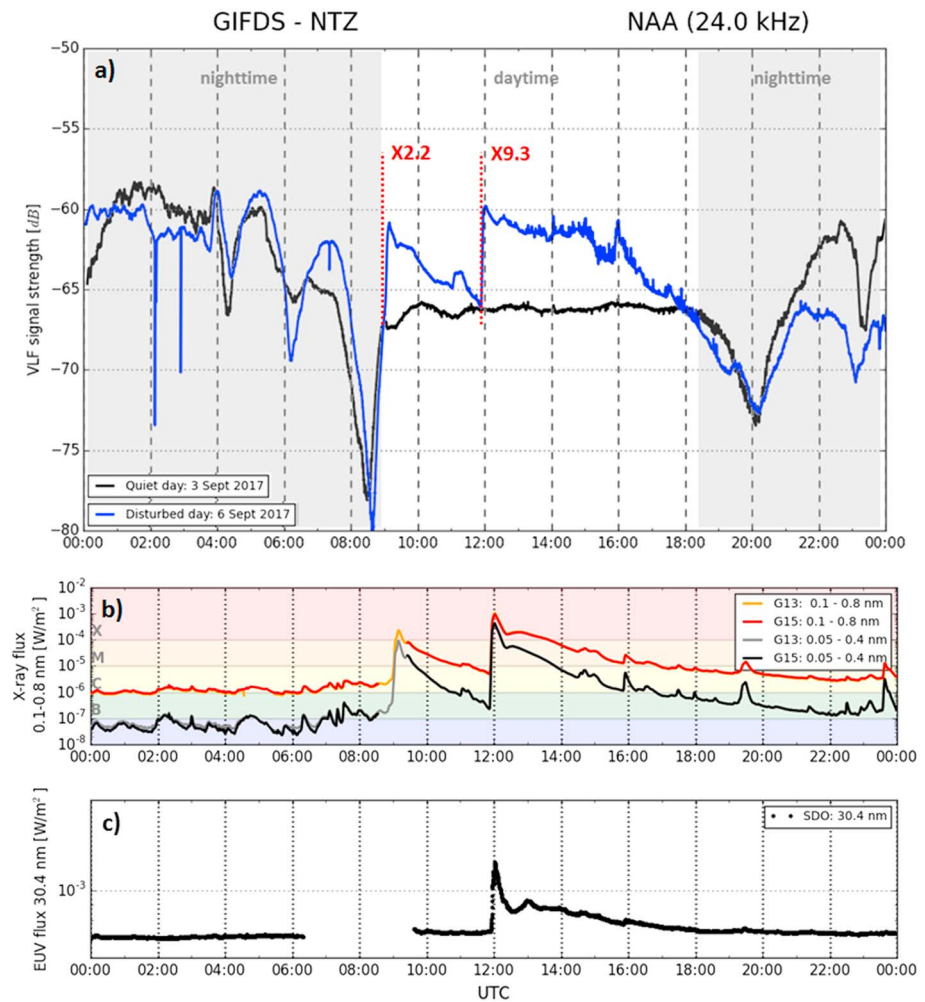


**Figure 2.** Flare activity on 6 September 2017 measured with three different instruments: (a) VLF amplitude measurements of Cutler NAA signals at 24.0 kHz (blue: disturbed day on 6 September 2017; black for comparison: quiet day on 3 September 2017) recorded by the GIFDS receiver at DLR Neustrelitz, (b) X-ray flux measured by the GOES satellites G15 (red: 0.1–0.8 nm; black: 0.05–0.4 nm) and G13 (red: 0.1–0.8 nm; gray: 0.05–0.4 nm), and (c) EUV flux at 30.4 nm provided by the Extreme Ultraviolet Variability Experiment onboard the Solar Dynamic Observatory satellite. VLF = Very Low Frequency; GIFDS = Global Ionospheric Flare Detection System.

signals propagate within the Earth-ionosphere waveguide, they contain valuable information about the dynamic bottomside ionosphere, which is disturbed during solar X-ray flares (Wenzel et al., 2016). Therewith, VLF measurements by Global Ionospheric Flare Detection System complement X-ray measurements by GOES, providing information about cause and effect on the ionosphere system.

So for both flares, the lower dayside ionosphere experienced an immediate response (a so-called sudden ionospheric disturbance) caused by the enhanced X-ray flux during solar flares. The X-ray measurements recorded by the primary (G15) and secondary (G13) GOES satellites are depicted in Figure 2b. Here we can distinguish between the two channels 0.1–0.8 nm (G15: red; G13: orange), indicating the well-known flare size in the X-ray range, and 0.05–0.4 nm (G15: black; G13: gray). Enhanced radiation during the strong X9.3 flare was not only examined in the X-ray but also in the EUV range (cf. Figure 2c). The EUV measurements by SDO illustrate a strong impact for 30.4 nm, primarily ionizing the *F* region (Handzo et al., 2014). Thus, a direct impact on GNSS measurements is expected. Please note that the EUV measurements by SDO during the time of the X2.2 flare were unfortunately not available. After the main activity period with the X9.3-flare as the maximum, a X8.2 and some minor flares occurred on 10 September before the third phase of decreasing activity occurred during 11 September till 13 September. In the following we will focus on the main event of this solar activity

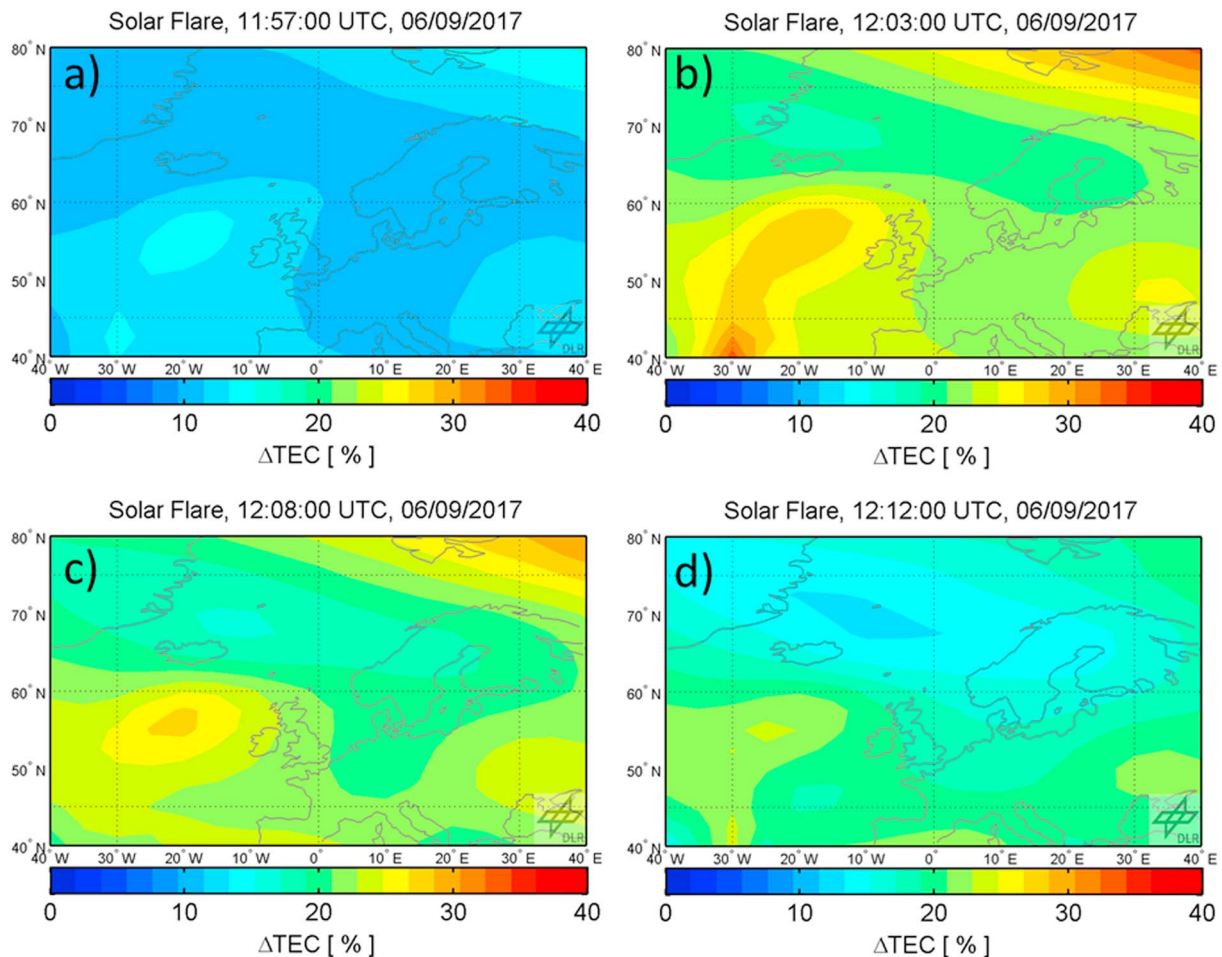


**Figure 3.** Direct impact of the X9.3 flare on the ionosphere using the difference between the real-time assimilated TEC map over Europe and the last TEC map before the flare, which is the TEC map produced at 11.53 UTC. TEC = Total Electron Content.

phase, the X9.3 flare, and follow its effect on the ionosphere down to application examples in the navigation domain.

## 2. Flare Effect on the Ionosphere Over Europe

The strongest flare event started on 6 September 2017 at 11:53 UT and ended at 12:10 with the maximum at 12:02 UT. The flare had a magnitude of X9.3 making it number 14 in the ranking of all flares observed by GOES so far. The last X-class flare of this order of magnitude occurred on 5 December 2006 more than a decade ago. The X9.3 flare had a strong effect on the ionosphere over the Central European region where the impact occurred about 2 P.M. in Central European Summer Time. At that time, the ionosphere usually reaches its maximum ionization over Central Europe within the diurnal cycle. In the following we will focus on the main X9.3 flare event and investigate its influence on the ionosphere and related performance degradation on navigation services in the aviation and maritime domain.

### 2.1. Data Processing

Ground-based data used within this publication are based on the International GNSS Service (IGS), the Ionosphere Monitoring and Prediction Center (Berdermann et al., 2014), and the high rate receiver network (EVNET; Noack et al., 2005). Data used within this paper are real-time measurements taken during the solar activity period. In case of the 1 Hz data from reference networks we used IGS Networked Transport of RTCM via Internet Protocol. Networked Transport of RTCM via Internet Protocol is a protocol developed by the Federal Agency for Cartography and Geodesy of Germany (BKG) that enables streaming of differential GNSS or Real-Time Kinematic (RTK) correction data in real time via the internet (Lenz, 2004). All data have been processed within the real-time data processing system of the Ionosphere Monitoring and Prediction Center to generate maps



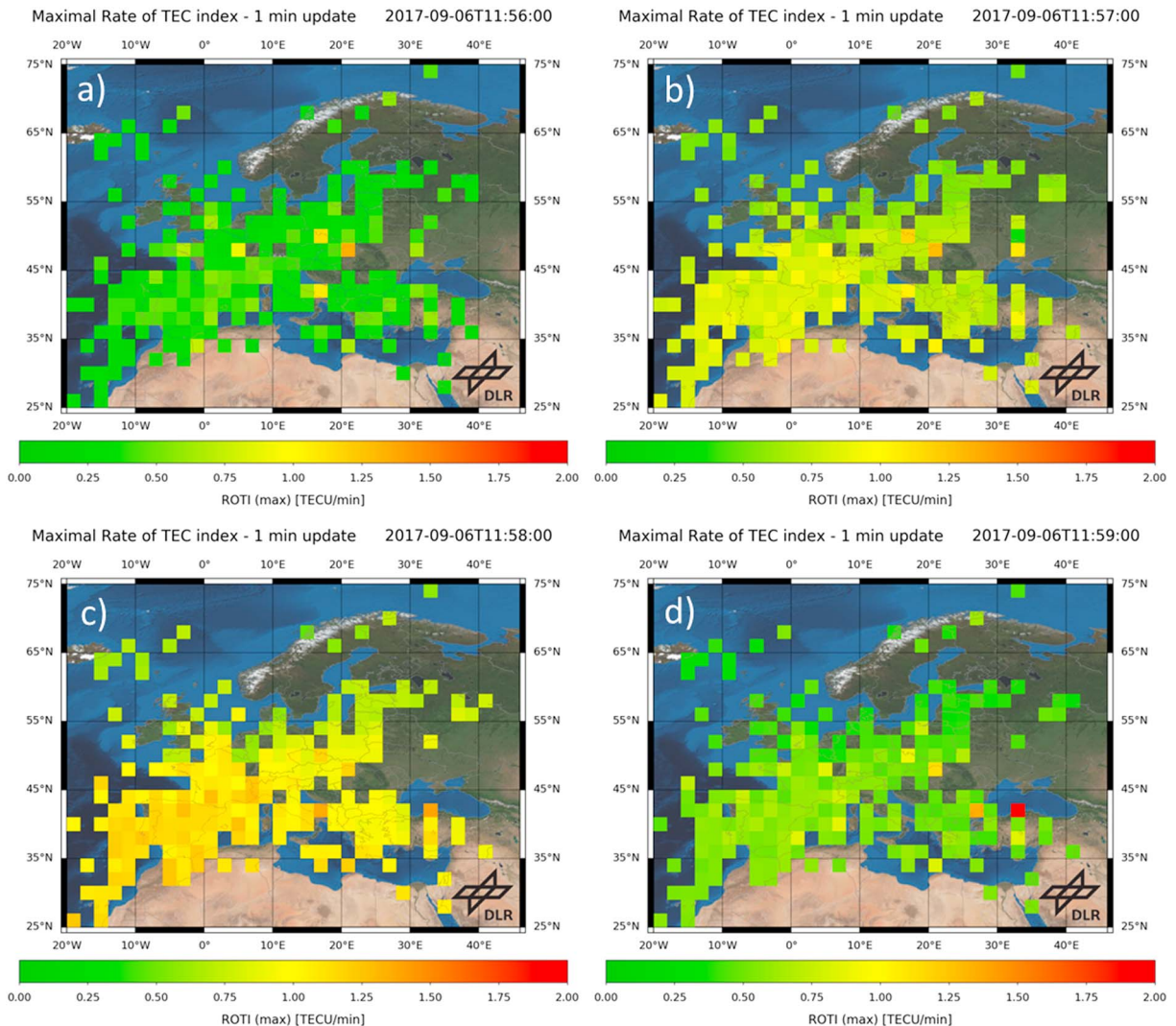


**Figure 4.** Shown are the direct impact of the X9.3 flare on the ionosphere in terms of a sudden increase and decrease of ROTI over Europe within 4 min (a)–(d) observed by Ionosphere Monitoring and Prediction Center's real-time ROTI processing system. TEC = Total Electron Content; ROTI = Rate Of TEC Index; TECU = TEC unit, 1 TECU =  $10^{16}$  electrons per square meter.

of the Total Electron Content (TEC; Jakowski, Mayer, et al., 2011) and the rate of change of TEC index (ROTI; Jacobsen, 2014; Pi et al., 1997), in order to investigate the dynamics in the ionosphere during the flare event. The TEC maps are generated using ground-based GNSS measurements assimilated into an empirical TEC model. The measurement data are preprocessed in order to derive calibrated slant TEC and to update the coefficients of the Neustrelitz TEC Model serving as ionospheric background. Subsequently, the calibrated slant TEC measurements are converted to vertical TEC (VTEC) using a single-layer mapping function for the shell-height of 400 km. Afterward VTEC is assimilated into the Neustrelitz TEC Model (Jakowski, Hoque, et al., 2011; Jakowski, Mayer, et al., 2011). Results are provided in TEC units (1 TECU =  $10^{16}$  electrons per square meter).

## 2.2. Data Interpretation

In Figures 3a–3d the difference between the real-time assimilated TEC maps in 5-min time steps and the TEC map just before the flare produced at 11.53 UTC is shown as reference. It becomes visible how the additional radiation component of the flare is producing a sudden increase in TEC within a very short time interval (from Figure 3a to 3b), which is decreasing after 12:03 UT (from Figure 3b to 3d). This could be seen as an indication that the additional ionospheric plasma generation due to the flare is caused in the lower layers of the ionosphere, where strong recombination processes occur, thus supporting the sudden decrease of ionospheric plasma after the flare event.

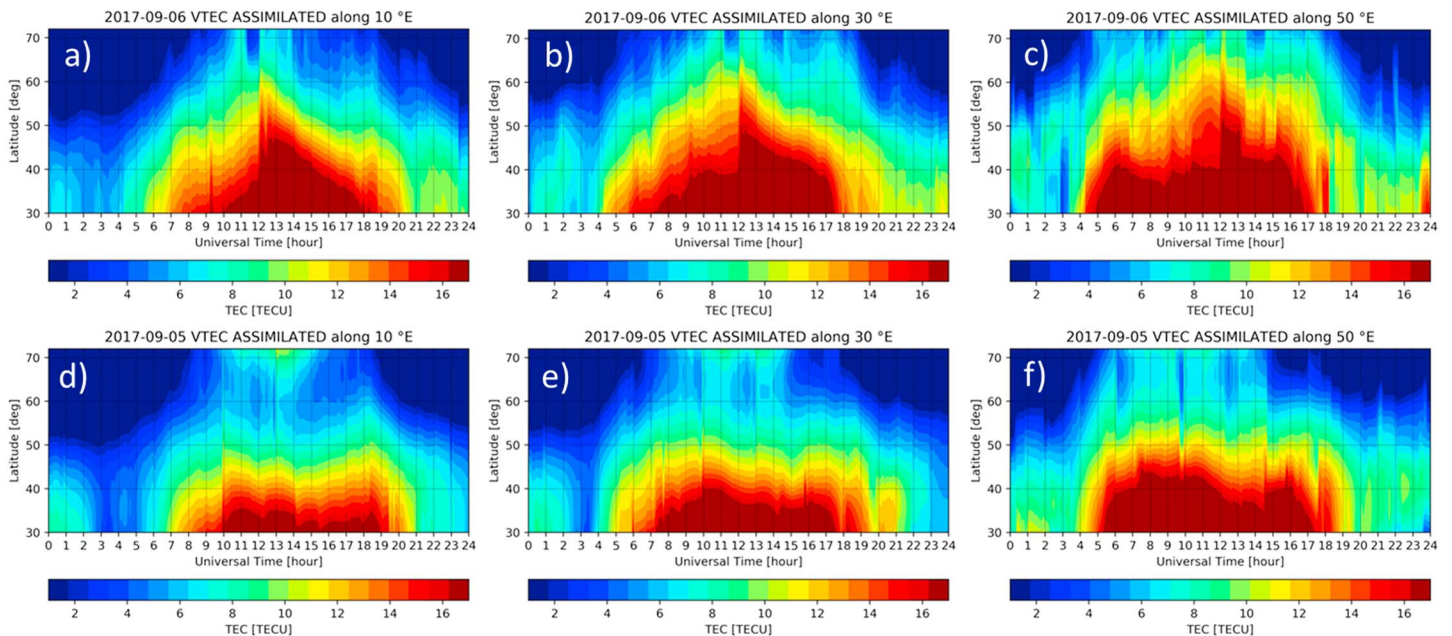


**Figure 5.** Ionospheric response over Europe to the X9.3 flare on 6 September 2017. The assimilated TEC values in the latitude band from 30 till 70°N for the longitudes 10, 30, and 50°E over the course of the day are shown in the top panels (a)–(c). In the bottom row the same plots of the previous day are given for comparison (d)–(f). TEC = Total Electron Content; VTEC = vertical TEC; TECU = TEC unit, 1 TECU =  $10^{16}$  electrons per square meter.

Similar observations can be made in the ROTI plots given in Figure 4. ROTI can be used as a measure to detect rapid changes of the ionospheric ionization. ROTI is calculated from real-time data stream at 1 min cadence from ground-based GNSS stations and mapped to the ionospheric pierce points. ROTI is sensitive to ionospheric perturbations and is usually used as a proxy for the S4 and  $\sigma_\phi$  indices derived from dual frequency high rate GNSS receiver data. S4 and  $\sigma_\phi$  indices describing amplitude and phase fluctuation of the received signal. The high resolution of ROTI allows studying the impact of the flare over Europe within 4 min. The whole dayside is affected as one can see in the sudden increase in ROTI from 11:56 till 11:59 UT. ROTI is typically used to identify small-scale ionospheric disturbances, but the flare event affects all used GNSS receivers due to the rapid change of the ionospheric conditions. Note that not the magnitude of TEC itself, but the sudden jump in TEC caused by strong changes in the ionosphere on a very short time scale causes problems for GNSS receiver, which are used for positioning, as we will see more in detail in section 3.

Figures 5a–5c show the effect of the X9.3 flare on the ionosphere for different longitudes to investigate the dependence on the solar incidence angle as described in Mendillo et al. (1974) and Hernandez-Pajares et al. (2012). All three plots show a significant increase in TEC during the flare impact with a rapid enhancement of ionization up to high latitudes. A solar dependence in longitude, which would indicate that the impact follows solar incidence conditions, cannot clearly be identified. Please note that the X2.2 flare, which occurred on the 6 September at the same day at 9:00 UT, also had a minor impact in  $\Delta$ TEC only visible as small peak at 10° and 30° plots.

In order to understand the differences in the ionosphere due to the direct flare impact, we show in Figures 5d–5f the previous day without X-flare activities for comparison. The increased TEC values visible at high latitudes during 5 September is due to ionospheric disturbances caused by increased solar wind conditions in connection with a CME arrival, as briefly discussed in section 1.

### 3. Implications for Navigation Services

In the following we discuss the impact of the flare-induced ionosphere changes on navigation and the positioning accuracy achievable by GNSS users (e.g., in the aviation and maritime transportation domain). In the following we choose four examples to demonstrate the solar flare effect on GNSS navigation services.

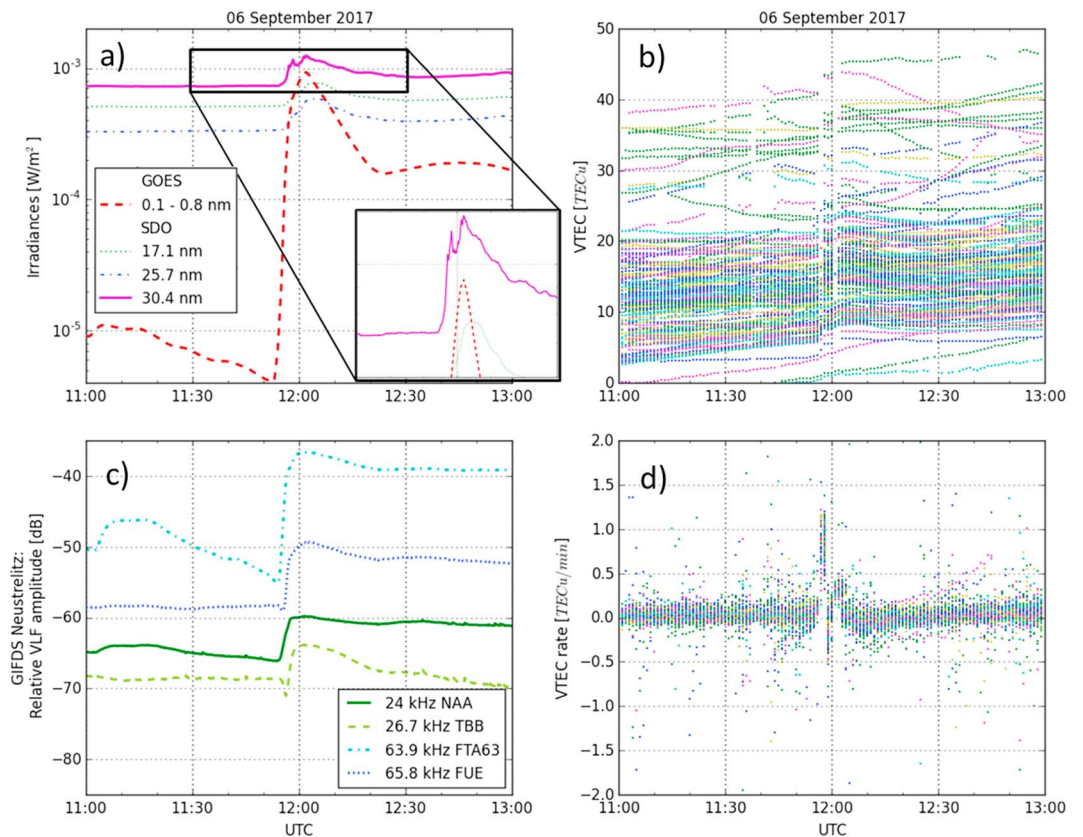


**Figure 6.** Shown is the progression curve of the X9.3 flare between 11:00 and 13:00 UT in different X-ray and EUV energy bands measured aboard SDO and GOES (a), with GIFDS (c), on changes in VTEC (b), and VTEC rate (d). GIFDS = Global Ionospheric Flare Detection System; VLF = Very Low Frequency; SDO = Solar Dynamic Observatory; VTEC = vertical Total Electron Content.

### 3.1. VTEC and Loss of Lock

In Figure 6a, we present the progression curve of the X9.3 flare for different energy bands compared to its influence on the ionosphere, illustrated by the changes in VTEC, as shown in Figure 6b. In the VTEC plot we used data only from IGS stations between 11:00 and 13:00 UT having a receiver to satellite link above 60° elevation piercing through the dayside ionosphere over Europe. The VTEC plots show two time periods around 11:58 and 12:02 UT, where most links to the satellite lost lock. Both periods are connected with the flare and are perfectly in line with both peaks visible in the 30 nm EUV band range of SDO. This supports former publications stating that TEC responses are especially well correlated with solar EUV flux enhancements in the 26–34 nm wavelength range (Hernandez-Pajares et al., 2012; Le et al., 2013; Tsurutani et al., 2005). Please note that solar flares are often accompanied by solar radio burst events, which can cause a similar effect on GNSS signal tracking performance for high solar radio flux levels at L-Band frequencies (Rodríguez-Bilbao et al., 2015). However, measured solar radio burst events with effect on GNSS performance during this space weather event do not coincide with the loss of lock intervals visible in the VTEC plots of Figure 6b. In the VTEC plot one can also see a few affected links around 11:35 not visible in the VTEC rate. The few affected links here are not related to the flare, but might result from other natural or technical effects. The impact of the flare, in particular the EUV component, causes an immediate increase of the ionospheric plasma visible in the related changes in the VTEC rate, see bottom right plot in agreement with ROTI observations seen in Figure 4. Both EUV peaks cause a strong dynamic in the bottomside ionosphere as we have discussed in section 2, leading to problems for GNSS receiver to maintain signal connection and in most cases to loose the links to the GNSS satellite, a so-called *loss of lock*.

### 3.2. Flare Effect on PPP Services

Navigation services based on the availability of timing information from multiple satellites experience a degradation in positioning accuracy. This issue is illustrated in Figure 7b, where the impact on the Precise Point



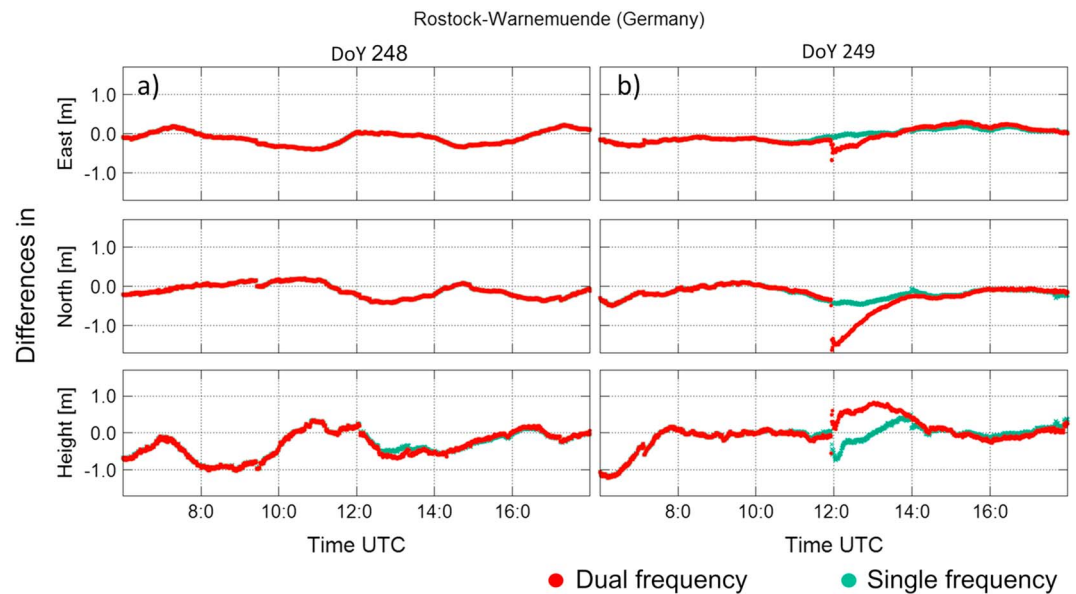


**Figure 7.** Shown on (b) are the impact of the X9.3 flare on single (green line) and dual frequency Precise Point Positioning (red line) positioning accuracy at the International Global Navigation Satellite System Service station WARN (LAT: 54.16978798; LONG: 12.10142406) in Rostock-Warnemünde (Germany). The plot shows the deviation in meter from reference coordinates calculated in 30 s intervals for East, North, and in the height direction. In (a) the same plot for the previous day is given, showing the nominal behavior.

Positioning (PPP) service is shown for single (green line) and dual frequency (red line) positioning. In Figure 7a the same plot for the previous day is given, showing the nominal behavior. The PPP plots in Figure 7 are based on GPS data from the station WARN in Rostock-Warnemünde (Germany) processed with the RTKLib framework to show as example the flare impact in the precise positioning domain. PPP is a phase-based GNSS-technique which has become popular in the last decade. In comparison to differential phase-based positioning techniques (like RTK), in PPP no observation data from a reference station are necessary (Zumberge et al., 1997). This has the advantage of no local restrictions, which makes this technique particularly suitable for maritime applications. Typical for PPP is a long convergence time to estimate the phase ambiguities. Furthermore, data corrections and models are needed to minimize all error influences in order to reach decimeter accuracy. In detail this means precise clock and orbit information have to be used, station depending effects like Earth tides need to be modeled and atmospheric effects in the troposphere and ionosphere must be taken into account. In the PPP-analysis we used the open source software RTKLib (<http://www.rtklib.com>) with the following data and settings: precise orbit and clocks (<ftp://cddis.gsfc.nasa.gov/gps/products/1966>), correction of the satellite antenna phase center offset (igs14\_1986.atx), troposphere estimation, and solid earth tides. In case of the single frequency solution IONEX files from the Center for Orbit Determination Europe are used.

The station WARN is situated in the midlatitude region of the ionosphere (LAT: 54.16978798; LONG: 12.10142406), where we can expect to see the solely effect of the flare without other overlapping disturbances as one can expect in the polar region due to the forcing from the geospace (Borries et al., 2015) or in the equatorial region caused by the daily formation of scintillation-effective ionospheric irregularities produced by the regular behavior of the low-latitude electrodynamics (Basu & Basu, 1981; Hlubek et al., 2014; Kriegel et al., 2017). In Figure 7b one can see how the single and dual frequency PPP is strongly affected during the flare event. The dual frequency positioning solution is even worse compared to the single frequency solution. The interruption started at 12:00 UT followed by the typical long convergence time after reinitialization until nominal accuracy conditions are reached again. Within the convergence time period strong deviations of the estimated position in East, North, and height direction of about 1 to 2 m occurred. We looked also into the Single Point Positioning error using RTKLib data from the IGS station WARN, but found a strong deviation of the order between 4 and 6 m masking the much smaller flare effect.

### 3.3. EGNOS

In the following we choose two examples to demonstrate the solar flare effect on GNSS navigation services. The first example is the European Geostationary Navigation Overlay Service (EGNOS; Ventura-Traveset &



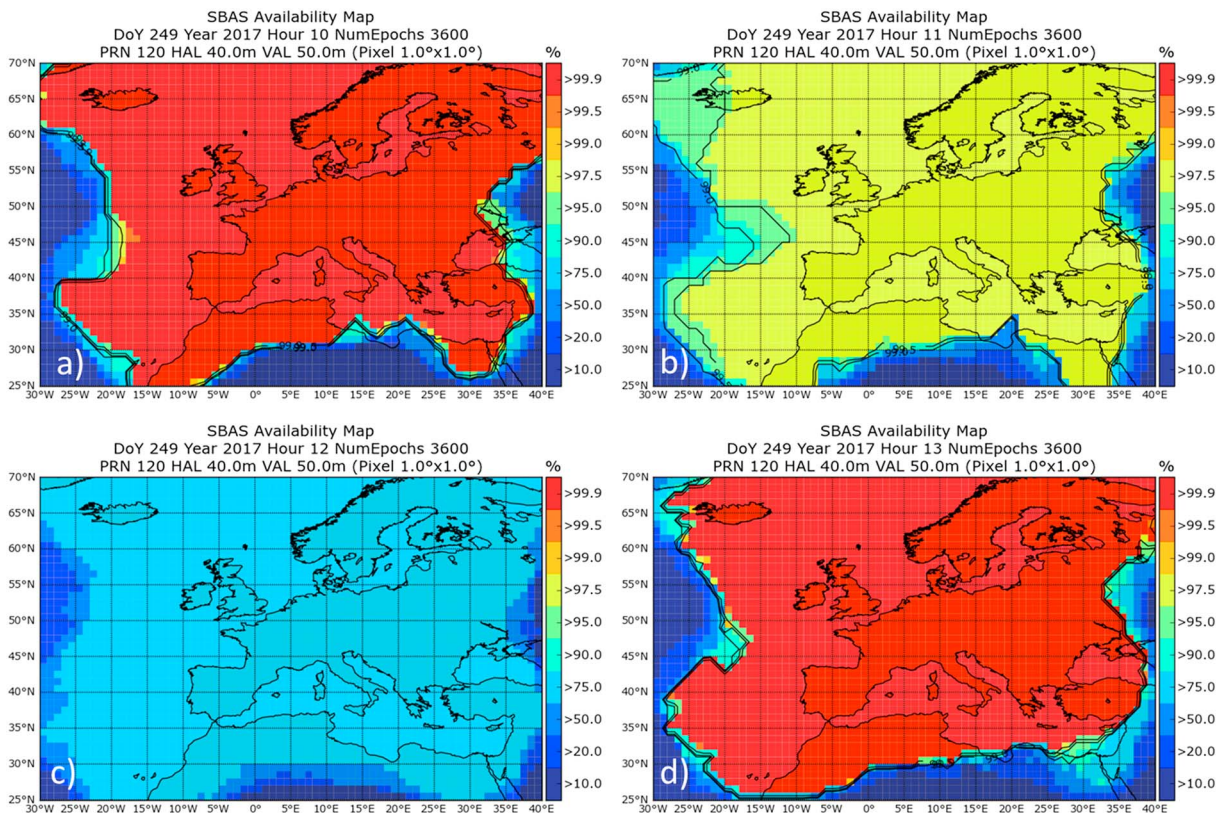


**Figure 8.** The hourly European Geostationary Navigation Overlay Service availability plots between 10:00 and 13:00 UT on 6 September are shown. The plots are generated with the ESA/UPC GNSS-Lab Tool (Sanz et al., 2012) and gracefully provided by ESA. Note in this figure red indicates high availability rates and blue indicates low availability rates. SBAS = satellite-based augmentation system.

Flament, 2006), which is the European regional satellite-based augmentation system. EGNOS provides safety of life navigation services to aviation, maritime, and land-based users. EGNOS is using GNSS measurements observed from precisely located reference stations within Europe and North Africa. The measurements are processed by a central computing center, where differential corrections and integrity messages are calculated. The calculation results are broadcasted for the covered area using geostationary satellites that serve as an augmentation, or overlay, to the original GNSS message.

During the X9.3 flare event, the EGNOS availability was significantly reduced as can be seen in the hourly EGNOS availability plots in Figures 8a–8d. Here the effect of both EUV peaks is clearly visible in the plot 8b from 11:00 till 11:59 UT caused by the first EUV peak at around 11:58 UT and in the plot Figure 8c from 12:00 to 12:59 UT with even stronger impact due to the second EUV peak at 12:02 UT leading to a strong decrease (10%) in the EGNOS availability. The availability is reduced over the full dayside region during this time to an amount, which might prevent the usage of EGNOS for safety of life applications, such as aircraft approach procedures based on localizer performance with vertical guidance, which in future shall become operationally equivalent to CAT I instrument landing system procedures. Please note that EGNOS availability plots are usually provided once at the end of the day (here hourly plots have been generated to highlight the flare effect). The users have no access to such information during the event. The only information important to them is if the system can be used or not. Therefore, loss of availability implies here that other backup navigation systems, like instrument landing system, are used instead.

### 3.4. AIS

The monitoring and assessment of vessel traffic is an important element of safe, secure, and efficient shipping. Collision and grounding avoidance at sea requires a reliable picture of the maritime traffic situation. The global trend toward more autonomous operations affects also the maritime world with its need of advanced, robust, and reliable systems in every situation. Some developments in this respect has been done with the introduction of the Automatic Identification System (AIS). This system improves the safety at sea, makes bridge

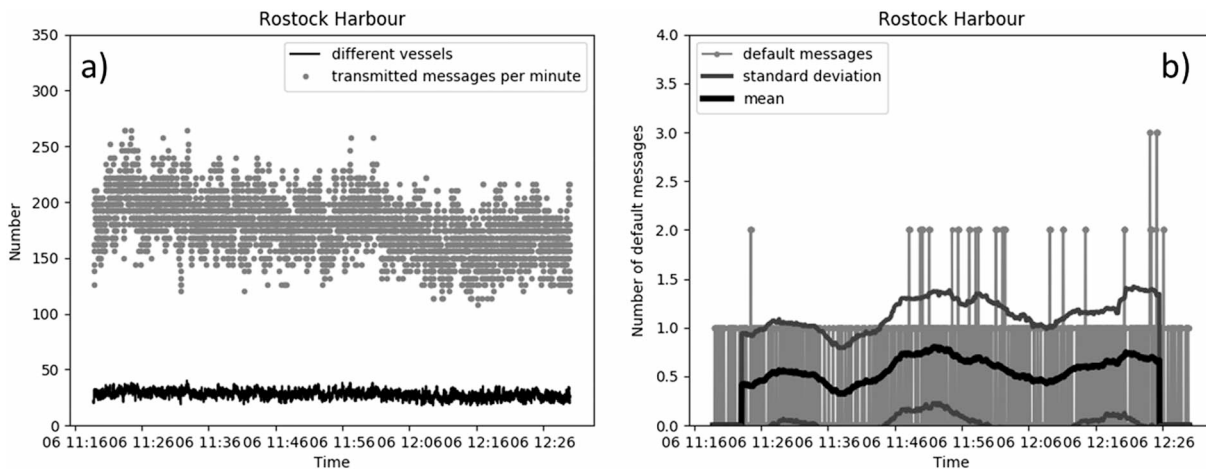


**Figure 9.** In panel (a) the statistic of the AIS system during the solar flare is shown, with the number of messages transmitted per minute (gray dots) and the number of different vessels in the reception area (solid black line). Panel (b) shows the number of faulty messages during this time. The solid black line is the mean value of a running average with a window size of 50 s, the dark gray solid lines show the standard deviation and the gray lines with dot describe the number of default messages within 0.1 s.

watchkeeping duties more comfortable, and enhances vessel traffic management ashore. Since AIS depends largely on GNSS, it is important to analyze a possible impact of natural disturbances, like solar flares, on the system. A previous analysis during quite space weather conditions indicate that about 1% of the transmitted AIS data at sea and about 10% in the harbor area show signs of implausibilities (Heymann et al., 2006).

Here we like to present a first brief look at possible solar flare manifestation on the AIS performance. In Figure 9a the statistic of the AIS system during the solar flare is given. The number of messages transmitted per minute depends on the traffic situation visible by the number of different vessels in the reception area. During the flare event 30 different vessels transmitted about 200 messages per minute. Figure 9b shows the number of faulty messages around the solar flare event. The gray lines with dot give the number of default messages within a 0.1 s time interval. The analysis of the AIS data show that the average number of default messages is in the order of 0.5 messages per 0.1 s with a standard deviation of 0.5. During the solar flare period there are several peaks exceeding the one sigma limit. Such increased AIS messaging traffic might indicate an enhancement of navigation information messages due to GNSS tracking problems. There is still a strong excess in the data after the flare event at 12:26. The most plausible explanation for this feature is that the ionospheric disturbance causes some longer lasting effect on the AIS transponder software, since there was no special vessel with faulty equipment or other obvious failure modes in this time frame.

#### 4. Conclusions

In the past decade the realization of our society to the fact that space weather poses a significant risk to our technological infrastructure has increased continuously. In many publications, (e.g., Borries et al., 2009, 2015; Förster & Jakowski, 2000; Lekshmi et al., 2011) the effect of space weather events has been analyzed focusing on the ionospheric response in respect to CMEs as the dominant threat. Recently, several authors focus especially on the positioning performance during ionospheric storms (e.g., Jacobsen & Andalsvik, 2016; Rodriguez-Bilbao et al., 2015). In this work we have analyzed the effects of the strong X9.3 flare on 6 September 2017, following its impact on the ionosphere and the resulting serious problems for precise positioning and GNSS navigation support services. Solar flares can affect navigation services for up to hours causing critical situations in many navigation applications. In particular, solar flares with a strong EUV component around 30 nm can seriously affect GNSS positioning services used in aviation and maritime navigation. We provided results from PPP during the strong solar flare compared to almost quiet conditions of the previous day to highlight the influence of solar flare events on GNSS positioning performance. We have shown that in addition to the PPP service also the EGNOS system, which provides safety of life navigation services to aviation, maritime, and land-based users, can be affected. Solar flares can lead to loss of signals at the GNSS receiver with significant effect on accuracy and integrity of the navigation performance. The AIS, a system introduced to improve the safety at sea, might be another possible service influenced during space weather events. We could identify a weak enhancement of AIS messages during the flare event, which might be an indicator for an increase

in GNSS navigation alert messages. A more detailed analysis of potential space weather impacts on AIS based on a solid statistic taking account different space weather events is planned. The impact of space weather events not only affects existing systems as we have shown, but are most probably also a threat for future technologies like autonomous car navigation. In addition to prepare for future severe or extreme space weather events, it is important to address the whole space weather interaction chain from the Sun to Earth with focus on impact to systems and services. This will allow us to get the needed knowledge of the vulnerability of our technological infrastructure to space weather events.

## Acknowledgments

We acknowledge the cooperation with the German Federal Agency for Cartography and Geodesy (BKG), the International GNSS Service (IGS), the NOAA Space Weather Prediction Center (SWPC), the World Data Center for Geomagnetism (WDC-2) Kyoto, and the GFZ Potsdam. We thank all institutions that host EVNet equipment: Bahir Dar University, JAXA, Swedish Institute of Space Physics, Stanford University, University of Tromsø, Universidad de La Laguna, Hartebeesthoek Radio Astronomy Observatory, University of Toulouse, EISCAT Ramfjordbotn. We kindly acknowledge the support for hosting GIGDS equipment from the Institute for Scientific Research at the Boston College, from the Institute for Nuclear Physics (PAN) in Krakow, Poland, from the Department of Aeronautics and Astronautics at Stanford University, and from the Center for Space and Remote Sensing Research, National Central University, Jungli, Taiwan. All data used within the publication are available from the long-term storage of the Institute of Communication and Navigation of the German Aerospace Center and are permanently provided via ftp access (SERVER: ftp.kn.nz.dlr.de, USER: dlr79, PASSWORD: 7uN3LaBZhebv) or on request to the email-address impc-uhd@dlr.de.

## References

- Baker, N., Li, X., Pulkkinen, A., Ngwira, C. M., Mays, M. L., Galvin, A. B., & Simunac, K. D. C. (2013). A major solar eruptive event in July 2012: Defining extreme space weather scenarios. *Space Weather*, 11, 585–591. <https://doi.org/10.1002/swe.20097>
- Basu, S., & Basu, S. (1981). Equatorial scintillations—A review. *Journal of Atmospheric and Terrestrial Physics*, 43, 472–489. [https://doi.org/10.1016/0021-9169\(81\)90110-0](https://doi.org/10.1016/0021-9169(81)90110-0)
- Berdermann, J., Jakowski, N., Hoque, M. M., Hlubek, N., Missling, K. D., Kriegel, M., et al. (2014). Ionospheric Monitoring and Prediction Center (IMPC). In *Proceedings of the 27th International Technical Meeting of The Satellite Division of the Institute of Navigation ION GNSS+* (pp. 14–21). Tampa, Florida.
- Borries, C., Berdermann, J., Jakowski, N., & Wilken, V. (2015). Ionospheric storms - A challenge for empirical forecast of the total electron content. *Journal of Geophysical Research: Space Physics*, 120, 3175–3186. <https://doi.org/10.1002/2015JA020988>
- Borries, C., Jakowski, N., & Wilken, V. (2009). Storm induced large scale TIDs observed in GPS derived TEC. *Annales de Geophysique*, 27(4), 1605–1612. <https://doi.org/10.5194/angeo-27-1605-2009>
- Chamberlin, P. C., Woods, T. N., Didkovsky, L., Eparvier, F. G., Jones, A. R., Machol, J. L., et al. (2018). Solar ultraviolet irradiance observations of the solar flares during the intense September 2017 storm period. *Space Weather*, 16. <https://doi.org/10.1029/2018SW001866>
- Eastwood, J. P., Biffis, E., Hapgood, M. A., Green, L., Bisi, M. M., Bentley, R. D., et al. (2017). The economic impact of space weather: Where do we stand. *Risk Analysis*, 37(2), 206–218.
- Förster, M., & Jakowski, N. (2000). Geomagnetic storm effects on the topside ionosphere and plasmasphere: A compact tutorial and new results. *Surveys in Geophysics*, 21(1), 47–87. <https://doi.org/10.1023/A:1006775125220>
- Gimenez de Castro, C. G., Raulin, J.-P., ValleSilva, J. F., Simoes, P. J. A., Kudaka, A. S., & Valio, A. B. (2018). The 6 September 2017 X9 super flare observed from submillimeter to mid-IR. *Space Weather*, 16, 1261–1268. <https://doi.org/10.1029/2018SW001969>
- Handzo, R., Forbes, J. M., & Reinisch, B. (2014). Ionospheric electron density response to solar flares as viewed by Digisondes. *Space Weather*, 12, 5–216. <https://doi.org/10.1002/2013SW001020>
- Hernandez-Pajares, M., Garcia-Rigo, A., Juan, J. M., Sanz, J., Monte, E., & Aragon-Angel, A. (2012). GNSS measurement of EUV photons flux rate during strong and mid solar flares. *Space Weather*, 10, S12001. <https://doi.org/10.1029/2012SW000826>
- Heymann, F., Noack, T., & Banyś, P. (2013). Plausibility analysis of navigation related AIS parameter based on time series. In *Proceedings of the European Navigation Conference*. Vienna.
- Hlubek, N., Berdermann, J., Wilken, V., Gewies, S., Jakowski, N., Wassaie, M., & Damtie, B. (2014). Scintillations of the GPS, GLONASS, and Galileo signals at equatorial latitude. *Journal of Space Weather and Space Climate*, 4, A22. <https://doi.org/10.1051/swsc/2014020>
- Jacobsen, K. S. (2014). The impact of different sampling rates and calculation time intervals on ROTI values. *Journal Space Weather Space Climate*, 4, A33. <https://doi.org/10.1002/2014SW0014031>
- Jacobsen, K. S., & Andalsvik, Y. L. (2016). Overview of the 2015 St. Patrick's day storm and its consequences for RTK and PPP positioning in Norway. *Journal of Space Weather and Space Climate*, 6, A9.
- Jakowski, N., Hoque, M. M., & Mayer, C. (2011). A new global TEC model for estimating transionospheric radio wave propagation errors. *Journal of Geodesy*, 85(12), 965–974.
- Jakowski, N., Mayer, C., Hoque, M. M., & Wilken, V. (2011). TEC models and their use in ionosphere monitoring. *Radio Science*, 46, RS0D18. <https://doi.org/10.1029/2010RS004620>, <http://www.agu.org/pubs/crossref/2011/2010RS004620.shtml>
- Kriegel, M., Jakowski, N., Berdermann, J., Sato, H., & Mersha, M. W. (2017). Scintillation measurements at Bahir Dar during the high solar activity phase of solar cycle 24. *Annales de Geophysique*, 35, 97–106.
- Le, H., Liu, L., Chen, Y., & Wan, W. (2013). Statistical analysis of ionospheric responses to solar flares in the solar cycle 23. *Journal of Geophysical Research: Space Physics*, 118, 576–582. <https://doi.org/10.1029/2012JA017934>
- Lekshmi, V. D., Balan, N., Tulasi, S. R., & Liu, J.-Y. (2011). Statistics of geomagnetic storms and ionospheric storms at low and mid latitudes in two solar cycles. *Journal of Geophysical Research*, 116, A11328. <https://doi.org/10.1029/2011JA017042>
- Lenz, E. (2004). Networked transport of RTCM via internet protocol (NTRIP) – Application and benefit in modern surveying systems. In *Proceedings FIG Working Week 2004*. Athens, Greece.
- Linty, N., Minetto, A., DAVIS, F., & Spogli, L. (2018). Effects of phase scintillation on the GNSS positioning error during the September 2017 storm at Svalbard. *Space Weather*, 16, 1317–1329. <https://doi.org/10.1029/2018SW001940>
- Mendillo, M., Klobuchar, J. A., Fritz, R. B., da Rosa, A. V., Kersley, L., Yeh, K. C., et al. (1974). Behavior of the ionospheric F region during the Great Solar Flare of August 7, 1972. *Journal of Geophysical Research*, 79(4), 665–672.
- Noack, T., Engler, E., & Klähn, D. (2005). High rate performance assessment of GNSS raw data based on the DLR experimentation and verification network. In *ION GNSS 2005* (pp. 573–583). Long Beach, CA (USA).
- Oughton, E. J., Skelton, A., Horne, R. B., Thomson, A. W. P., & Gaunt, C. T. (2017). Quantifying the daily economic impact of extreme space weather due to failure in electricity transmission infrastructure. *Space Weather*, 15, 65–83. <https://doi.org/10.1002/2016SW001491>
- Pi, X., Mannucci, A. J., Lindqwister, U. J., & Ho, C. M. (1997). Monitoring of global ionospheric irregularities using the worldwide GPS network. *Geophysical Research Letters*, 24(18), 2283–2286. <https://doi.org/10.1029/97GL02273>
- Redmon, R. J., Seaton, D. B., Steenburgh, R., He, J., & Rodriguez, J. V. (2018). September 2017's geoeffective space weather and impacts to Caribbean radio communications during hurricane response. *Space Weather*, 16, 1190–1201. <https://doi.org/10.1029/2018SW001897>
- Riley, P. (2012). On the probability of occurrence of extreme space weather events. *Space Weather*, 10, S02012. <https://doi.org/10.1029/2011SW000734>
- Riley, P., & Love, J. J. (2017). Extreme geomagnetic storms: Probabilistic forecasts and their uncertainties. *Space Weather*, 15, 53–64. <https://doi.org/10.1002/2016SW001470>
- Rodriguez-Bilbao, I., Radicella, S. M., Rodriguez-Caderot, & Herraiz, M. (2015). Precise point positioning performance in the presence of the 28 October 2003 sudden increase in total electron content. *Space Weather*, 13, 698–708. <https://doi.org/10.1002/2015SW001201>



- Sanz, J., Rovira-Garcia, A., Hernandez, M., Juan, J., Ventura-Traveset, J., Lopez, C., & Hein, G. (2012). The ESA/UPC GNSS-Lab Tool (gLAB): An advanced educational and professional package for GNSS data processing and analysis. In *6th ESA Workshop on Satellite Navigation Technologies Multi-GNSS Navigation Technologies*. Noordwijk, Netherlands.
- Schrijver, C. J., Kauristie, K., Aylward, A. D., Denardini, C. M., Gibson, S. E., Glover, A., et al. (2015). Understanding space weather to shield society: A global road map for 2015–2025 commissioned by COSPAR and ILWS. *Advances in Space Research*, 55(12), 2745–2807.
- Tsurutani, B. T., Judge, D. L., Guarnieri, F. L., Gangopadhyay, P., Jones, A. R., Nuttall, J., et al. (2005). The October 28, 2003 extreme EUV solar flare and resultant extreme ionospheric effects: Comparison to other Halloween events and the Bastille Day event. *Geophysical Research Letters*, 32, L03S09. <https://doi.org/10.1029/2004GL021475>
- Ventura-Traveset, J., & Flament, D. (Eds.) (2006). *EGNOS - The European Navigation Overlay System - A cornerstone of Galileo*. Noordwijk, Netherlands: ESA Publications Division, ESTEC.
- Wenzel, D., Jakowski, N., Berdermann, J., Mayer, Chr., Valladares, C., & Heber, B. (2016). Global ionospheric flare detection system (GIFDS). *Journal of Atmospheric and Solar-Terrestrial Physics*, 138, 233–242.
- Zumberge, J., Heflin, M., Jefferson, D., Watkins, M., & Webb, F. (1997). Precise point positioning for the efficient and robust analysis of GPS data from large networks. *Journal of Geophysical Research*, 102(B3), 5005–5017.